

# On Phase Distribution and Phase Transformations in Phosphoric Irons Studied by Metallography

GADADHAR SAHOO and R. BALASUBRAMANIAM

The microstructures of novel phosphoric irons have been studied by metallography in order to understand the phase distribution and phase transformations in the iron-rich end of the Fe-P phase diagram. Both Nital etchant and Oberhoffer's reagent were effective in revealing dual-phase microstructures of phosphoric irons that were heat treated in the ( $\alpha + \gamma$ ) region. The phase distribution in dual-phase microstructures was analyzed by quantitative metallography and related to the phase diagram. The morphology of austenite depended on phosphorus content and heat-treatment temperature. The microsegregation of phosphorus and phosphorus diffusivity was studied as a function of the temperature and soaking time of the specimens. The beneficial effect of the heat treatment of phosphoric irons in the dual-phase region of the Fe-P phase diagram on mechanical behavior has been confirmed by tensile testing.

DOI: 10.1007/s11661-007-9227-1

© The Minerals, Metals & Materials Society and ASM International 2007

## I. INTRODUCTION

THE Gupta-period Delhi Iron Pillar is a living testimony to the high level of skill achieved by ancient Indian ironsmiths in the extraction and processing of iron. This Pillar has attracted the attention of engineers, especially corrosion technologists, because it has withstood corrosion for more than 1600 years. The presence of relatively high phosphorus (0.25 wt pct) in the forge-welded Pillar plays a major role in its excellent corrosion resistance.<sup>[1,2]</sup> Phosphorus facilitates the formation of a protective passive film on the surface, which provides the Pillar its exceptional corrosion resistance properties. Recently, the remarkable corrosion resistance of phosphoric irons (containing up to 0.5 wt pct phosphorus) has been demonstrated in aggressive concrete environments.<sup>[3,4]</sup> Recognizing the annual economic loss due to corrosion in both developed and developing nations, it is important to study the possible use of phosphorus-containing steels in modern applications.

Phosphorus in steel leads to "cold shortness," due to the phosphorus segregation at the grain boundaries. However, carbon can replace phosphorus from the grain boundaries by the site competition effect, when Fe-P alloys contain a low amount of carbon.<sup>[5,6]</sup> Fe-P alloys containing 0.01 to 0.05 wt pct carbon have exhibited good ductility.<sup>[7,8]</sup> Moreover, improved mechanical properties have been reported for vacuum-melted pure Fe-P alloys, after suitable control of the microstructure.<sup>[8]</sup>

The control of the microstructure is important in realizing ductile phosphoric irons. The phase diagram of Fe-P provides some ideas for heat-treating Fe-P alloys of low P content to render them ductile. The Fe-P alloy with P content in the range of 0.0 through 0.68 wt pct (Figure 1(a), reported by Kubaschewski<sup>[9]</sup> for pure Fe-P alloys) and 0.0 through 0.57 wt pct (Figure 1(b), reported by Vogel<sup>[10]</sup> for samples containing impurities) reveal austenite of lower phosphorus content at the grain boundaries of ferrite after heat-treating in the two-phase ( $\alpha + \gamma$ ) region. This inhomogeneity of P created at a high temperature persists even at room temperature. Therefore, the heat treatment of phosphoric irons of low P content will open several possibilities regarding microstructures and phase distribution; one of the aims of this article is to address these issues in novel phosphoric irons.

The other aspect of the study was to realize good mechanical properties after heat treatment in the two-phase ( $\alpha + \gamma$ ) region, to highlight the fact that ductile phosphoric irons can be obtained. Considering the good corrosion resistance they exhibit in concrete environments,<sup>[3,4]</sup> phosphoric irons are candidate materials for concrete reinforcement applications.

## II. EXPERIMENTAL PROCEDURE

Phosphoric irons of three different phosphorus contents, namely, P<sub>1</sub>, P<sub>2</sub>, and P<sub>3</sub>, were prepared through an ingot casting route after melting in a high-frequency induction-melting furnace (175 KW, 1000 Hz) in air. The alloys were prepared from calculated amounts of soft iron (Fe-0.001C) and Fe-P mother alloys (Fe-22P), depending on the required phosphorus content. The carbon content was controlled to about 0.02 wt pct by the addition of mild steel scrap containing 0.16 pct carbon. The ingots were soaked at 1150 °C for 4 hours, primarily to remove macrosegregation in ingots and

GADADHAR SAHOO, formerly Doctoral Student, Department of Materials and Metallurgical Engineering, Indian Institute of Technology, is Assistant Manager, R&D Center for Iron and Steel, Steel Authority of India Limited, Ranchi 834002, India. R. BALASUBRAMANIAM, Professor, is with the Department of Materials and Metallurgical Engineering, Indian Institute of Technology, Kanpur 208016, India. Contact e-mail: bala@iitk.ac.in

Manuscript submitted August 10, 2006.

Article published online July 6, 2007.

then forged into round bars 26 and 16 mm in diameter. The chemical compositions of P<sub>1</sub>, P<sub>2</sub>, and P<sub>3</sub> were analyzed by using direct reading optical emission spectrometer (OES) in triplicate. The composition ranges are specified in Table I. The phosphorus contents of P<sub>1</sub>, P<sub>2</sub>, and P<sub>3</sub> (reported in Table I) were determined by wet-chemical analysis.

Specimens of P<sub>1</sub>, P<sub>2</sub>, and P<sub>3</sub> were heat treated at different temperatures in the  $\gamma$ -loop and the  $(\alpha + \gamma)$  dual-phase region of the Fe-P phase diagram (Figure 1) and later examined microscopically. The details of heat treatments are summarized in Table II. In each case, the samples were air cooled after the heat treatment. Samples P<sub>2</sub> and P<sub>3</sub> were homogenized in the ferrite region prior to heat treatment in the  $(\alpha + \gamma)$  dual-phase region. The fractions of austenite and ferrite phases were estimated as a function of time, *i.e.*, 0.25, 1, 4, and 12 hours at 1100 °C, in the case of P<sub>2</sub> and P<sub>3</sub>.

The etching reagents used in optical microscopy were 3 pct Nital (3 pct HNO<sub>3</sub> in ethanol) and Oberhoffer's reagent. The Oberhoffer's reagent was prepared by mixing 500 mL H<sub>2</sub>O + 30 g FeCl<sub>3</sub> + 0.5 g SnCl<sub>2</sub> + 1 g CuCl<sub>2</sub> + 500 mL C<sub>2</sub>H<sub>5</sub>OH + 50 mL HNO<sub>3</sub>.<sup>[8]</sup>

Triplicate tensile tests were performed at room temperature (27 °C) in a 20-kN capacity tensile machine using a strain rate of  $1.6 \times 10^{-3} \text{ s}^{-1}$ . This strain rate lies in the regime for "static" tension test, as defined by Dieter.<sup>[11]</sup> The tensile specimens were prepared from hot-forged phosphoric irons, P<sub>1</sub>, P<sub>2</sub>, and P<sub>3</sub>, 26 mm in diameter according to ASTM 370. After failure, the percentage reduction in the area and the percentage elongation at failure were estimated from the specimens, while the lower yield strength and ultimate tensile strength were determined from the engineering stress-strain curves.

### III. RESULTS AND DISCUSSION

#### A. Phase Distribution

Figure 2(a) shows micrographs of hot-forged, as-received specimen P<sub>1</sub> along the transverse direction after etching with Nital. Only ferrite grains, without any "ghosting" features, were observed. However, in the case of the hot-forged specimen P<sub>2</sub> (Figure 2(b)) and P<sub>3</sub> (Figure 2(c)), ghosting features were revealed. The ghost

Table I. Chemical Composition of Phosphoric Irons (Weight Percent) Obtained by Triplicate Testing

Sample	C	P	Si	Mn	S	Ni	Cr	Mo	V	Cu
P <sub>1</sub>	0.021	0.105	0.023	0.043	0.016	0.026	0.043	0.003	0.003	0.033
	to	to	to	to	to	to	to	to	to	to
P <sub>2</sub>	0.035	0.126	0.036	0.049	0.018	0.027	0.045	0.007	0.003	0.033
	to	to	to	to	to	to	to	to	to	to
P <sub>3</sub>	0.036	0.340	0.026	0.052	0.018	0.027	0.050	0.004	0.004	0.037
	to	to	to	to	to	to	to	to	to	to
P <sub>3</sub>	0.019	0.480	0.022	0.064	0.022	0.026	0.056	0.003	0.003	0.038
	to	to	to	to	to	to	to	to	to	to
	0.021	0.500	0.033	0.071	0.025	0.026	0.057	0.004	0.006	0.039

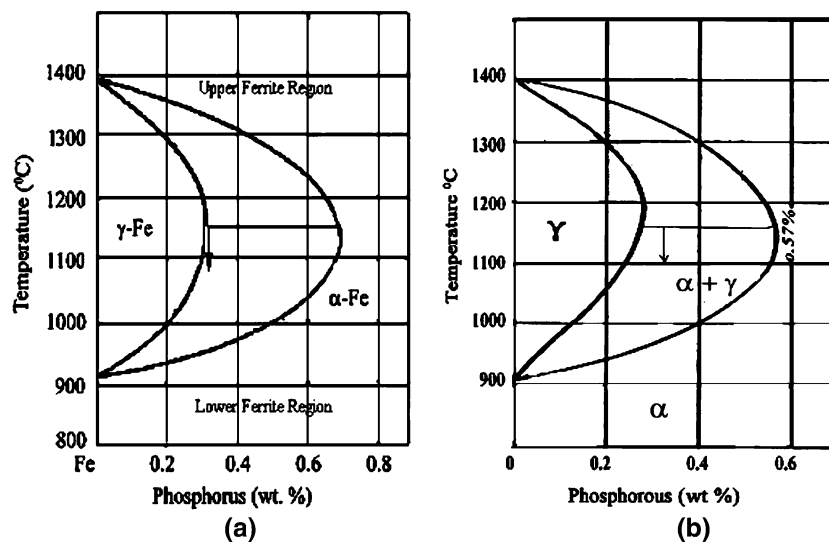


Fig. 1—High-temperature  $\gamma$ -loop and  $(\alpha + \gamma)$ -loop region of Fe-P phase diagram: (a) per Kubaschewski<sup>[9]</sup> and (b) per Vogel.<sup>[10]</sup> Tie-lines have been drawn for the temperatures investigated. The arrow indicates iron with 0.32 pct P.

**Table II. Details of Heat Treatments Conducted on Phosphoric Iron Specimens for Varying Soaking Times at Different Temperatures; in Each Case, Samples Were Air Cooled after Soaking**

Samples	Homogenization Temperature and Time of Soaking in Ferrite Region	Time of Soaking (Hours) in ( $\alpha + \gamma$ ) Dual-Phase Region			
		Time of Soaking at 930 °C (h)	Time of Soaking at 1000 °C (h)	Time of Soaking at 1100 °C (h)	Time of Soaking at 1180 °C (h)
P <sub>1</sub>	—	0.25, 0.5	—	—	—
P <sub>2</sub>	900 °C and 0.25, 0.5, 1, 2, 4, 8, and 16 h	—	—	—	—
P <sub>2</sub>	8 h	—	0.25, 0.5	0.25, 0.5	—
P <sub>3</sub>	1000 °C, 4 h	—	—	—	—
P <sub>3</sub>	1000 °C, 12 h	—	—	0.25, 0.5	—
P <sub>3</sub>	1300 °C, 2 h	—	—	—	0.25

Note: Samples heat treated at different temperatures in dual-phase region were first homogenized according to the second column.

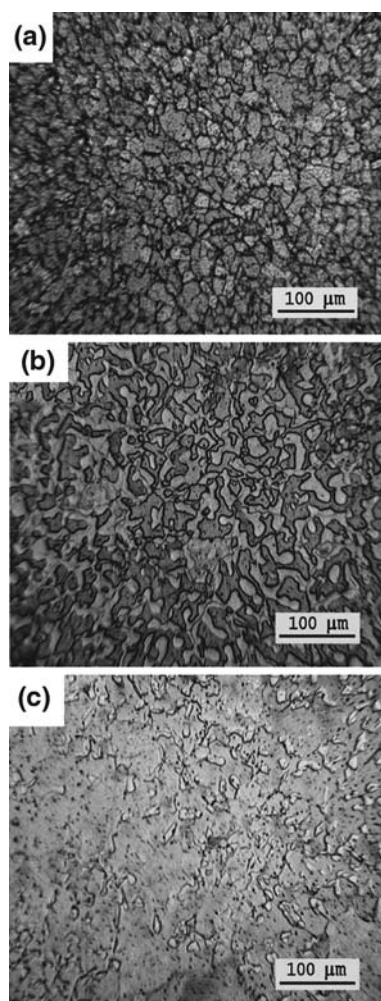


Fig. 2—Optical micrographs of as-received specimens after etching with Nital: (a) P<sub>1</sub> showing only ferrite grains, (b) P<sub>2</sub>, and (c) P<sub>3</sub> showing ghosting microstructure of prior austenite and prior ferrite.

lines are boundaries of sharp change in the local phosphorus content in the ferrite matrix that result from the presence of prior austenite along the grain boundaries of prior ferrite. The low-phosphorus region,

indicating a prior austenite region, etches preferentially, giving rise to a surface relief.<sup>[12]</sup>

The as-received specimen P<sub>1</sub> was hot forged in the austenite region (*i.e.*, inside the  $\gamma$ -loop), which later transformed to ferrite upon cooling. The phosphorus content in the ferrite was uniformly distributed, as all the material was austenite in the austenite region. Therefore, ghosting features were not observed in P<sub>1</sub>. On the other hand, P<sub>2</sub> and P<sub>3</sub> were forged after soaking the ingot in the dual-phase ( $\alpha + \gamma$ ) region. This resulted in the formation of austenite at the grain boundaries of ferrite.

Optical micrographs of as-received specimens P<sub>2</sub> and P<sub>3</sub> after etching with Oberhoffer's reagent are shown in Figures 3(a) and (b). The distribution of prior phases was revealed more clearly, when compared to samples etched with Nital. The prior austenite regions, containing lower phosphorus content, appear in light contrast using Nital etchant and in dark contrast with Oberhoffer's reagent.<sup>[4,13]</sup> Therefore, this dual-phase heat treatment resulted in removing phosphorus away from the grain boundaries of ferrite.

In order to understand the time scale involved for the phosphorus microsegregation to be removed, samples of P<sub>2</sub> were soaked for different times at 900 °C (which is in the single-phase ferrite region of the Fe-P phase diagram<sup>[9,10]</sup>) and their microstructures were observed. After soaking specimens of P<sub>2</sub> for 8 hours, the contrast between the prior phases was negligible. After 16 hours of soaking, there was no contrast observed. This was due to the homogenization of the phosphorus distribution by diffusion. This homogenization treatment has been discussed in detail elsewhere.<sup>[4,13]</sup>

In order to optimize the soaking time for obtaining the equilibrium dual-phase distribution, the as-received sample of P<sub>2</sub> was heat treated in the dual-phase region for different times. The volume fractions of prior austenite in heat-treated (and air-cooled after soaking at 1100 °C for 0.25, 1, 4, and 12 hours) specimens of P<sub>2</sub> are provided in Table III. This was almost 55 to 60 pct. The volume fraction of prior austenite remained almost constant with the time of soaking. This indicated that there was an equilibrium distribution of austenite and ferrite in the ( $\alpha + \gamma$ ) dual-phase region during the

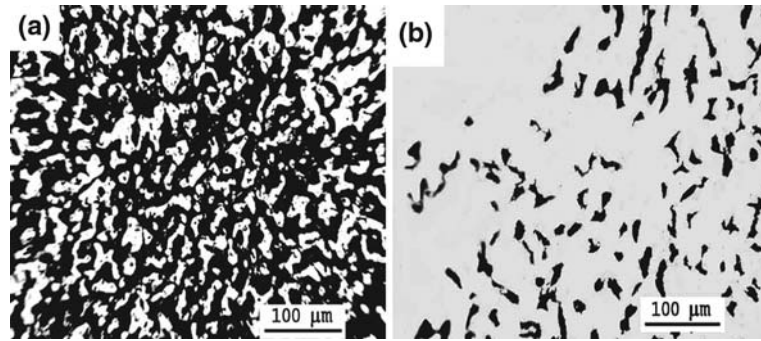


Fig. 3—Optical micrographs of as-received specimens: (a)  $P_2$  and (b)  $P_3$  obtained along transverse direction, after etching with Oberhoffer's reagent. Dark areas indicate low-phosphorus regions (*i.e.*, regions of prior austenite) and light regions indicate high-phosphorus regions (*i.e.*, regions of prior ferrite).

**Table III. Volume Fraction (Percent) of Prior Austenite in Air-Cooled Specimen  $P_2$  after Soaking at 1100 °C for Different Times**

Field	Soaking Time (Hours)			
	0.25	1	4	12
1	52	60	56	57
2	59	61	54	55
3	54	59	49	60
4	56	60	50	56
5	60	50	53	50
Average	57	58	54	56
Standard deviation	3	4	3	3

**Table IV. Volume Fraction (Percent) of Prior Austenite in Normalized Specimen  $P_3$  after Soaking at 1100 °C for Different Times**

Field	Soaking Time (Hours)			
	0.25	1	4	12
1	28	34	16	15
2	31	33	31	21
3	33	17	30	2
4	26	20	17	5
5	18	35	25	1
Average	27	28	24	9
Standard deviation	6	9	7	9

soaking of the ingot for 4 hours at 1150 °C, prior to forging. This is the required soaking time, which can be followed in commercial practice prior to rolling for keeping a bare minimum level of phosphorus at grain boundaries.

The phase distribution noted in  $P_2$  can be understood from the Fe-P phase diagram (Figure 1). From these figures, it can be noticed that for  $P_2$  (considering 0.32 pct as average phosphorus content), the fractions of phases at 1150 °C remain almost constant at that level at 1100 °C, according to the lever rule. Applying the lever rule to the tie-line drawn at 1100 °C in the phase diagram proposed by Kubaschewski,<sup>[9]</sup> in Figure 1(a), the volume fractions of austenite can be calculated as 95 pct and that of ferrite as 5 pct. The austenite volume fraction estimated from the phase diagram (Figure 1(b)) determined by Vogel<sup>[10]</sup> was 86 pct. The deviation observed in the present study from the phase diagrams may be due to the inward shifting of the  $\gamma$ -loop and ( $\alpha + \gamma$ ) regions due to the presence of impurities such as Mo, Cr, C, *etc.* However, the phase diagram suggested by Vogel<sup>[10]</sup> provided better correlation with the present experimental observations.

The fraction of the prior austenite phase in the optical micrographs of  $P_3$  (Figures 2(c) and 3(b)) were relatively lower than that noticed in  $P_2$ ; this is because of the higher phosphorus content in  $P_3$ . To determine whether this phase distribution in  $P_3$  (which was obtained after soaking the ingot  $P_3$  for 4 hours) was in equilibrium, specimens of  $P_3$  were further soaked for 0.2, 1, and

12 hours at 1100 °C. The estimated volume fractions of the prior phases (Table IV) indicated a decreasing trend of the volume fraction of austenite as a function of the soaking time. This suggested that the phosphoric iron  $P_3$  required more than 12 hours to attain the equilibrium distribution of phases at 1100 °C.

Considering 0.49 pct as the average phosphorus content for  $P_3$ , and utilizing the phase diagram proposed by Vogel, the volume fraction of equilibrium austenite at 1100 °C was estimated to be 25 pct. This is higher than that obtained by quantitative metallography (9 pct). The volume fraction of austenite estimated from the phase diagram suggested by Kubaschewski (Figure 1(a)) was 52 pct, which is significantly different from that obtained by quantitative metallography (9 pct). The phase diagram proposed by Kubaschewski may be inappropriate for the phosphoric irons in this study, since it is based on data from pure F-P alloys. The homogenization of the P content in sample  $P_3$  was also studied by heat treating the sample at both the lower ferrite region (1000 °C) and upper ferrite region (1300 °C). Homogenization was achieved faster at 1000 °C (in just 4 hours) for  $P_3$  than for  $P_2$  at 900 °C. Similarly, in the case of the sample soaked for only 2 hours at 1300 °C, a single-phase ferrite microstructure without any ghosting features was observed after etching with Nital. This suggested that soaking ingots (prior to rolling) in the upper ferrite region will be faster and, thus, a comparable amount of energy can be saved.



## B. Phase Transformations

The microstructure observed in  $P_2$  after soaking at 1000 °C for 15 minutes is shown in Figure 4. It reveals that the austenite nucleated at the grain boundaries of ferrite as both grain-boundary austenite allotriomorphs and Widmanstätten needles. The microstructure in Figure 4(b) was obtained from the region “A” in Figure 4(a) at higher magnification. It revealed grain-boundary austenite allotriomorphs and some isolated blocks of prior austenite inside the grain. Impurity particles are the nucleation sites for these isolated blocks of prior austenite that grow from the interior of the grain, and these are known as intragranular Widmanstätten needles or plates.<sup>[13]</sup> The microstructure in Figure 4(c) was obtained from region “B” in Figure 4(a) at higher magnification. It revealed austenite of the Widmanstätten-needle type. The local phosphorus

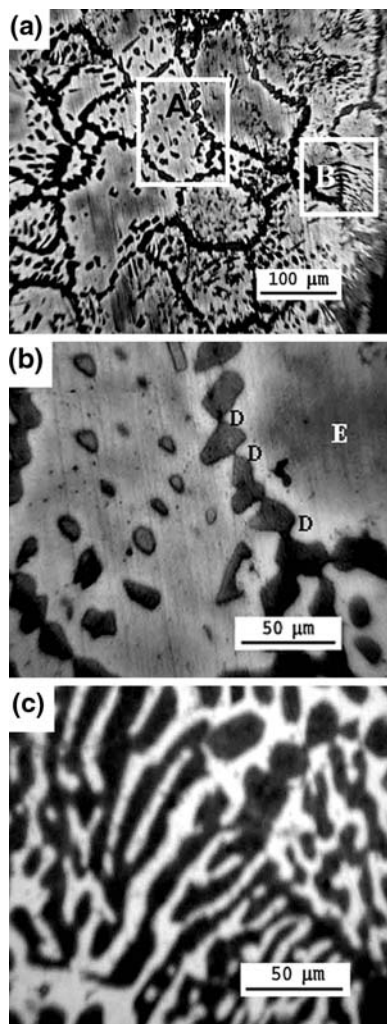


Fig. 4—Optical micrographs (b) revealing grain-boundary austenite allotriomorphs and isolated austenite blocks at higher magnification at the region “A” in micrograph (a) of  $P_2$  (soaked for 15 minutes at 1000 °C), and micrograph (c) revealing Widmanstätten needles at higher magnification at the region “B” in micrograph (a). Region “D” in micrograph (b) indicates phosphorus-enriched “white halo” around austenite allotriomorph, and “E” indicates low-phosphorus-content ferrite at the dual-phase ( $\alpha + \gamma$ ) region.

enrichment in the ferrite around the prior austenite phase boundary was revealed by a light halo around the prior austenite. This is indicated as “D” in the micrograph shown in Figure 4(b). This partitioning of phosphorus is analogous to the microsegregation that arises due to the rejection of the solute to the vicinity of dendrites during the formation of primary and secondary dendrites, in the process of solidification.<sup>[14]</sup> As austenite possesses a lower solubility of phosphorus, it rejects phosphorus during its formation at the grain boundaries of ferrite. This occurs when heat treatment is performed in the dual-phase region. The enriched phosphorus at the austenite-ferrite interface region did not have sufficient time to diffuse into the interior region of the grain, which was comparatively depleted of phosphorus. This interior low-phosphorus region is indicated as “E” in Figure 4(b).

While similar phosphorus partitioning was noticed for the  $P_1$  specimens soaked for 0.25 hours at 930 °C, a sharp contrast in the duplex microstructure along with spheroidized and coarsened austenite was obtained in the case of the longer period of heat treatment at 930 °C (more than 0.5 hours) and the heat treatment at the higher temperature (950 °C).

Similarly, soaking  $P_2$  and  $P_3$  at 1100 °C for 15 and 30 minutes, the austenite Widmanstätten needles and allotriomorphs were spheroidized and thickened, and the white halo of enriched phosphorus around the austenite disappeared. This is due to the faster diffusion of phosphorus from the enriched region into the grain interior at the higher temperature. Attempts were also made to observe the morphology of the austenite during nucleation and growth after homogenizing the  $P_3$  specimen in the upper ferrite region (1300 °C) of the ( $\alpha + \gamma$ ) dual-phase region in the Fe-P phase diagram. This homogenized specimen was air cooled after soaking for 15 minutes at 1180 °C. The microstructure of this sample (Figure 5) shows nucleation of the austenite with allotriomorph morphology at the ferrite grain boundaries. There was no white halo region around the austenite. The microstructure also revealed that the size of the prior ferrite grain was larger than in any other case so far discussed. This is because of the grain growth

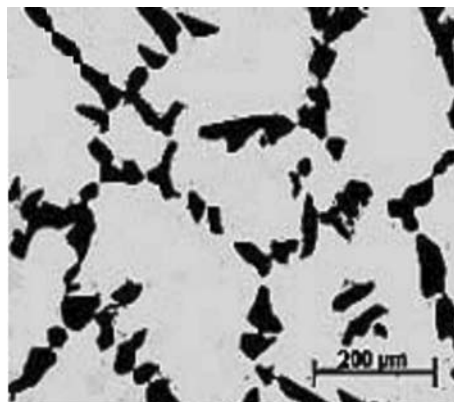


Fig. 5—Optical micrographs of  $P_3$  soaked for 15 minutes at 1180 °C, showing grain-boundary austenite allotriomorphs.

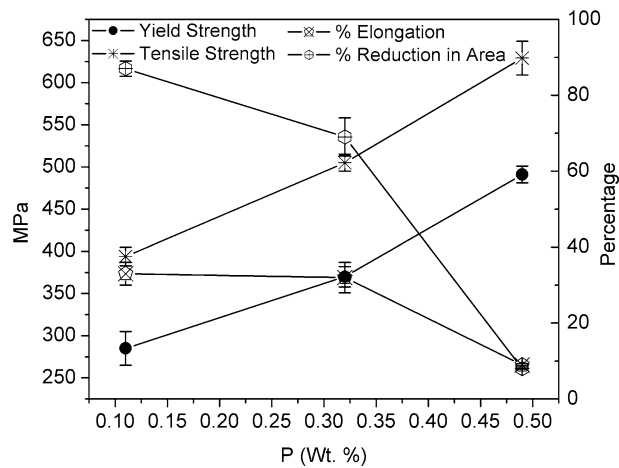


Fig. 6—Mean values of mechanical properties (with error bars) of phosphoric iron  $P_1$ ,  $P_2$ , and  $P_3$ . Ultimate tensile stress (\*) and yield stress (●) increased with increasing P content, while pct reduction in area (⊕) and pct elongation (⊗) decreased with increasing P content.

in the ferrite during the homogenization treatment at the higher temperature (1300 °C).

### C. Mechanical Properties

The beneficial effect of soaking phosphoric irons at 1150 °C for 4 hours prior to forging, specifically, removing phosphorus away from the grain-boundary regions, has been confirmed by metallography. It is, therefore, anticipated that the deleterious effect of phosphorus will not be evident. The mechanical properties of phosphoric irons were evaluated after soaking and the subsequent forging operation at 1150 °C.

The mean mechanical properties of phosphoric irons  $P_1$ ,  $P_2$ , and  $P_3$  are graphically shown as bar diagrams in Figure 6. Error bars are provided to indicate the standard deviation. The yield stress and ultimate tensile stress increased with increasing phosphorus content. The percentage elongation and percentage reduction in the area at failure decreased with increasing phosphorus content. Specimen  $P_3$  failed after yielding, unlike other samples. The percentage of elongation and the percentage of reduction in the area at failure were significantly low for this sample (Figure 6). This increase in strength and decrease in ductility with increasing phosphorus concentration can be attributed to the strong solid-solution strengthening effect of phosphorus.<sup>[10]</sup> The ductility of  $P_2$  was almost the same as that of  $P_1$ . The volume fraction of the prior austenite in  $P_2$  (Table III) was higher than that present in  $P_3$  (Table IV). A higher amount of phosphorus was kept away from the grain boundaries in the case of  $P_2$ , due to the heat treatment in the duplex region. The beneficial effect of the dual-phase region heat treatment was further realized from the poor ductility of homogenized and single-phase ferrite structure phosphoric iron  $P_2$ .<sup>[4]</sup> The effect of phosphorus on the mechanical

properties is in line with the data found in the literature.

## IV. CONCLUSIONS

This is the first study on phosphoric irons containing impurities similar to that present in mild steel. Phosphoric iron  $P_1$ ,  $P_2$ , and  $P_3$  soaked in the ( $\alpha + \gamma$ ) region in a Fe-P phase diagram revealed a dual-phase microstructure after etching with Nital and Oberhoffer's reagent. The beneficial effect of this dual-phase heat treatment, which resulted in the formation of low-phosphorus-content austenite at the grain boundaries of ferrite, has been demonstrated by tensile testing. The soaking time required to obtain this equilibrium dual-phase distribution was optimized in the case of  $P_2$ . Grain-boundary allotriomorphs, Widmanstätten needles, isolated blocks of prior austenite, and a phosphorus-enriched region around the grain-boundary allotriomorphs were present in  $P_2$  and  $P_3$  after soaking for a short period in the ( $\alpha + \gamma$ ) dual-phase region. Providing homogenization treatment to phosphoric irons prior to rolling will be faster in an upper ferrite region and will save energy. The tensile properties of phosphoric irons  $P_1$  and  $P_2$  were comparable to that of mild steel.

## ACKNOWLEDGMENT

The authors acknowledge the Field Gun Factory (Kanpur, India) for forging the phosphoric irons and completing the composition analysis.

## REFERENCES

1. R. Balasubramaniam: *Corr. Sci.*, 2000, vol. 42, pp. 2103–29.
2. R. Balasubramaniam and A.V. Ramesh Kumar: *Corr. Sci.*, 2000, vol. 42, pp. 2085–2101.
3. R. Balasubramaniam and G. Sahoo: *Corrosion Resistant Phosphoric Iron for Concrete Embedment and Reinforcement*, Indian Patent Application Number 1823/Del/2005.
4. G. Sahoo: Doctoral Thesis, Indian Institute of Technology, Kanpur, India, 2006.
5. H. Erhart and H.J. Grabke: *Scripta Metall.*, 1981, vol. 15, pp. 531–34.
6. S. Suzuki, K. Abiko, and H. Kimura: *Trans. ISIJ*, 1985, vol. 25, pp. 62–68.
7. B.E. Hopkins and H.R. Tipler: *J. Iron Steel Inst.*, 1958, vol. 188, pp. 218–37.
8. J.W. Stewart, J.A. Charles, and E.R. Wallach: *Mater. Sci. Technol.*, 2000, vol. 16, pp. 283–90.
9. O. Kubaschewski: *Iron—Binary Phase Diagrams*, Springer-Verlag, Berlin, 1982, pp. 84–86.
10. R. Vogel: *Arch Eisenhüttenwes.*, 1929, vol. 3, pp. 369–81.
11. G.E. Dieter: in *Mechanical Metallurgy*, SI Metric ed., McGraw Hill, Newark, NJ, 1988, pp. 295 and 558.
12. J.L. Haughton: *J. Iron Steel Inst.*, 1927, vol. 115, pp. 417–33.
13. J.W. Stewart, J.A. Charles, and E.R. Wallach: *Mater. Sci. Technol.*, 2000, vol. 16, pp. 291–302.
14. V. Singh: *Physical Metallurgy*, Standard Publisher Distributor, Delhi, 1999, pp. 278–88.